



# Effect of synthesis technique on electrochemical performance of bismuth selenide

Zulfiqar Ali, Chuanbao Cao\*, Jili Li, Yanli Wang, Tai Cao, M. Tanveer, Muhammad Tahir, Faryal Idrees, Faheem K. Butt

Research Centre of Materials Science, School of Materials Science and Engineering, Beijing Institute of Technology, Beijing 100081, People's Republic of China

## H I G H L I G H T S

- First attempt of using thermoelectric materials in LIB to tackle thermal runaway.
- $\text{Bi}_2\text{Se}_3$  rectangular nanosheets (BRNS) were prepared by thermochemical method.
- Self assembled nanosheets (SANS) were prepared by hydrothermal method.
- First discharge capacity is  $725.6 \text{ mAh g}^{-1}$  for BRNS and  $419.6 \text{ mAh g}^{-1}$  for SANS.
- Intercalation and replacement reaction were suggested during battery operation.

## A R T I C L E I N F O

### Article history:

Received 26 August 2012

Received in revised form

27 November 2012

Accepted 28 November 2012

Available online 5 December 2012

### Keywords:

Semiconductors

Bismuth selenide

Rectangular nanosheets

Self assembled nanosheets

Lithium ion batteries

## A B S T R A C T

In this work we propose a novel idea of using thermoelectric material in lithium ion batteries. The reason behind this idea is to improve the efficiency of batteries especially when heat dissipation and exothermic reaction of cathode and anode with the electrolyte at higher temperatures restricts their continuous operation due to thermal runaway. In order to execute this idea we develop a new synthetic technique for fabrication of  $\text{Bi}_2\text{Se}_3$  (thermoelectric material) and also compare its efficiency by preparing this material by existing synthetic technique. Charge/discharge comparison of both the samples indicate that the synthesis technique has a profound effect on electrochemical performance. Bismuth selenide ( $\text{Bi}_2\text{Se}_3$ ) is intentionally selected for this purpose.  $\text{Bi}_2\text{Se}_3$  rectangular nanosheets (BRNS) with thicknesses of 200–500 nm are synthesized by a simple thermochemical method in which we use bismuth and selenium powders as precursors. Self assembled nanosheets (SANS) in spherical shape are prepared by conventional hydrothermal technique. Charge discharge experiments show that BRNS synthesized with this technique have reasonable performance as compared to nanosheets synthesized by conventional hydrothermal technique. It shows that first discharge capacity is up to  $725.6 \text{ mAh g}^{-1}$  for BRNS and  $419.6 \text{ mAh g}^{-1}$  for SANS.

© 2012 Elsevier B.V. All rights reserved.

## 1. Introduction

The temperature of a lithium ion cell is determined by the heat balance between the amount of heat generated and that dissipated by the cell. The heat generation follows exponential function while the heat dissipation keeps linear function. When a cell is heated above a certain temperature (usually above  $130\text{--}150^\circ\text{C}$ ), exothermic chemical reactions between the electrodes and electrolyte set in will raise its internal temperature. If the cell can dissipate this heat, its temperature will not rise abnormally. However, if the heat generated is more than what can be dissipated, the exothermic processes

would proceed under adiabatic-like conditions and the cell's temperature will increase rapidly. This rising temperature will further accelerate the chemical reactions, rather than the desired galvanic reactions, causing even more heat to be produced, eventually resulting in thermal runaway [1]. It is proposed that above  $80^\circ\text{C}$ , thermal runaway can occur spontaneously as a result of fire or explosion [2]. Similarly at temperatures lower than  $0^\circ\text{C}$  batteries exhaust rapidly. These two phenomena introduce a very small range of temperatures for battery operation especially for hybrid electric vehicles (HEV) and electric vehicles (EV).

We develop an idea to overcome this issue, i.e. using thermoelectric materials in batteries. The thermoelectric effect is the direct conversion of temperature differences to electric voltage and vice-versa. A thermoelectric device creates a voltage when a temperature difference is introduced and vice versa. Conversely, when

\* Corresponding author. Tel.: +86 10 68913792; fax: +86 10 68912001.  
E-mail address: [cbcao@bit.edu.cn](mailto:cbcao@bit.edu.cn) (C. Cao).

a voltage is applied to it, it creates a temperature difference. At the atomic scale, an applied temperature gradient causes charge carriers in the material to diffuse from the hot point to the cold point. This effect can be used to enhance conductivity, measure or change the temperature of an object. Because the direction of heating and cooling is determined by the polarity of the applied voltage, hence thermoelectric devices fabricated from thermoelectric materials are efficient temperature controllers without using circulating fluid. It is also a fact that the rate performance of electrochemical materials can be improved by enhancing the ionic/electronic conductivity.

Bismuth chalcogenides such as  $\text{Bi}_2\text{Te}_3$  and  $\text{Bi}_2\text{Se}_3$  comprise some of the best performing room temperature thermoelectric [3–10] with a temperature independent thermoelectric effect, therefore suitable for refrigeration applications. Nanostructures growth of such materials will exhibit the interesting physical and chemical properties [11–13]. Since tellurium is very rare as compared to selenium so in order to execute our idea we have synthesized Bismuth selenide for application in lithium ion batteries. It is worth mentioning here that bismuth selenide has prospective applications in thermoelectric, electrochemical hydrogen storage, optoelectronic devices, and IR spectroscopy etc [15–22].

Although electrochemical hydrogen storage properties of  $\text{Bi}_2\text{Se}_3$  have been reported [14,15] but there are no reports for electrochemical lithium ion properties as anode material. The consideration of unsuitability near some researchers might be a reason for this. In order to tackle this issue we have synthesized bismuth selenide by different techniques and studied the effect of synthetic technique on electrochemical performance because this is a fact that the experimental conditions are important for the surface states, which mainly control the properties of  $\text{Bi}_2\text{Se}_3$  and are modified by chemical reactions under ambient conditions [23]. Therefore, main purpose of this study was to investigate the effect of synthesis technique of  $\text{Bi}_2\text{Se}_3$  on electrochemical behavior for application in lithium ion batteries.

A number of synthesis techniques have been reported to control the morphology of  $\text{Bi}_2\text{Se}_3$  nanostructures, such as microwave-assisted technique for nanosheets [24], the sonoelectrochemical or template-assisted method for nanowires [25,26], co-reduction method under ultrasonic irradiation for nanobelts [27] and the hydrothermal co-reduction or solvothermal method for nanotubes, nanorods and nanoflakes [28–30]. However, these techniques are either complex or expensive. Recently, there have been a number of reports published for nanostructures growth of  $\text{Bi}_2\text{Se}_3$  by CVD technique using  $\text{Bi}_2\text{Se}_3$  compound as the starting material [31–33].  $\text{Bi}_2\text{Se}_3$  is an expensive material; there is a need to develop a cost effective, simple and novel technique to synthesize  $\text{Bi}_2\text{Se}_3$  nanosheets. We have used Bi and Se elements as starting materials in alumina boat and successfully controlled the morphology of  $\text{Bi}_2\text{Se}_3$ .

Electrochemical performance of Bismuth selenide for application in lithium ion batteries has never been reported earlier. We have prepared  $\text{Bi}_2\text{Se}_3$  by different syntheses techniques and measured its lithium ion battery capacity for the first time ever. Also  $\text{Bi}_2\text{Se}_3$  Rectangular nanosheets (BRNS) have never been synthesized by this novel strategy to date to the best of our knowledge. Charge discharge experiments show that the first cycle discharge capacity is  $725.6 \text{ mAh g}^{-1}$  for BRNS.

## 2. Experimental

### 2.1. Synthesis of BRNS

Bismuth and selenium powders were engaged as starting materials. These powders were mixed in (1:1) ratio and grinded in

mortar for 30 min. About 1 g of the mixture was loaded in small rectangular alumina boat. The furnace was pumped out using a mechanical rotary pump for removing the residual air contents from the furnace tube and then also flushed heavily with high purity argon gas for about 30 min. Later on argon gas flow was adjusted at 50 sccm (standard cubic centimeter per minute) and the furnace was switched on to reach the first target temperature ( $t_1$ ) of  $700^\circ\text{C}$  at ramp rate of  $5^\circ\text{C min}^{-1}$  and kept there for 30 min, then it was cooled at the same rate to reach the second target temperature ( $t_2$ ) of  $530^\circ\text{C}$ , it was maintained for a reaction time of 120 min and then furnace was cooled down naturally. A dark gray color product was obtained from the alumina boat and preserved in airtight plastic boxes for further investigations.

### 2.2. Synthesis of SANS

SANS were synthesized by conventional hydrothermal technique. All chemical reagents were of analytical grade and used without further purification. In a typical synthesis procedure, solution A was prepared by continuous stirring a mixture of 20 ml ethylene glycol (EG) and 30 ml oleic acid (OA) with 0.972 g of  $\text{Bi}(\text{NO}_3)_3 \cdot 5\text{H}_2\text{O}$ . Solution B was prepared by mixing 0.237 g Se in 4 ml of nitric acid ( $\text{HNO}_3$ ). Then solution B was mixed with solution A. The mixture was transferred into a 60 ml Teflon-lined autoclave. The autoclave was sealed, maintained at  $180^\circ\text{C}$  for 20 h, and cooled to room temperature naturally. The precipitates were collected and washed with absolute ethanol and distilled water several times. Then the sample was dried in a vacuum at  $60^\circ\text{C}$  for several hours.

### 2.3. Structural and morphological characterizations

The structure and the phase purity of the products was determined by X-ray powder diffraction (XRD, Philips X'Pert Pro MPD) with  $\text{Cu K}\alpha$  radiation ( $\lambda = 0.15406 \text{ nm}$ ) whereas the morphologies of the products were examined by scanning electron microscopy (SEM, Hitachi S-3500). The chemical composition of the product was investigated by EDS.

### 2.4. Electrochemical measurements

Electrochemical properties of  $\text{Bi}_2\text{Se}_3$  powder were measured by fabricating CR2025 coin cells. A solution containing 5 wt.% polyvinylidene fluorides (PVDF) in 1-methyl-2-pyrrolidinone (NMP) as a binder was added to the mixture to form paste. This paste containing  $\text{Bi}_2\text{Se}_3$ , carbon and PVDF in 75:20:5 weight ratios respectively was coated onto copper foils to form working electrodes and dried for 12 h in vacuum at  $120^\circ\text{C}$ . Lithium metal was used as counter electrode and Celgard 2400 film as separator. The electrolyte was 1 M  $\text{LiPF}_6$  in a mixture of ethylene carbonate (EC) and dimethyl carbonate (DMC) (1:1, v/v).

Cell assembling was carried out in an argon-filled glove box (M Braun 100 G, Germany), where water and oxygen concentration was kept less than 1 ppm. The coin cells were charged/discharged to different Li contents and voltage with a current of  $50 \text{ mA g}^{-1}$ . A Li foil pressed into Ni net served as the counter and reference electrodes. The scan potential ranges were in the range of 0.02–3.0 and 1.6–3.0 V (versus  $\text{Li/Li}^+$ ), and the potential scanning rate was  $0.5 \text{ mV s}^{-1}$ .

## 3. Results and discussion

Fig. 1(a) shows the XRD pattern of BRNS synthesized in furnace tube using bismuth and selenium powders as precursors. From this figure, all the characteristic peaks correspond to pure  $\text{Bi}_2\text{Se}_3$ . Miller indices of every peak are indexed in the Fig. 1. The main peaks

located at  $2\theta = 29.3736, 40.2576, \text{ and } 43.6783^\circ$  correspond to (015), (1010) and (110) planes respectively, have the highest intensity. All the peaks match well with the peaks of rhombohedral  $\text{Bi}_2\text{Se}_3$ . The lattice parameters calculated for  $\text{Bi}_2\text{Se}_3$  are  $a = 4.1368 \text{ nm}$  and  $c = 28.6342 \text{ nm}$ , which are correspond to the standard values of JCPDS card No.33-0214 for  $\text{Bi}_2\text{Se}_3$ .

Fig. 1(b) shows XRD spectrum of SANS synthesized by conventional hydrothermal process. It can be seen that phase obtained by hydrothermal process is almost same as obtained by CVD method. It can be inferred from the comparison that our product is single phase pure  $\text{Bi}_2\text{Se}_3$ .

Purity of the product was further investigated by (EDS) analysis. Fig. 2 represents the result of energy dispersive X-ray spectroscopic (EDS) investigation of the as-synthesized products. (EDS) results of BRNS are presented in Fig. 2(a) which depicts that the product is highly pure bismuth selenide. The bismuth and selenium are present in 71.20:28.80. EDS spectra for SANS are given in Fig. 2(b) which suggests that Bi and Se are present in 87.69:12.31 ratios. This difference in elemental ratios is due to the difference in synthesis techniques.

Fig. 3 presents the Scanning Electron Microscopy (SEM) micrographs of the as synthesized products. The product mainly consists of nanosheets. Fig. 3(a) represents the SEM images of the product at  $20 \mu\text{m}$  scale. Fig. 3(b) presents the SEM micrographs at  $10 \mu\text{m}$  scale. In order to observe morphology clearly, SEM micrographs were taken at higher resolution scales as presented in Fig. 3(c) and (d). Nanosheets seem to be rectangular in shape. Thickness of the nanosheets was estimated from these images to be in the range of  $200\text{--}500 \text{ nm}$  while the lengths are in micrometers scale as indicated in Fig. 3(c). Fig. 3(d) represents that some portion of the product was not converted to BRNS, temperature gradient is considered to be the major reason for this difference in morphology.

Fig. 4 shows that product synthesized by conventional hydrothermal technique. Product mainly consists of nanosheets self assembled in spherical shape. Fig. 4(a) and (b) represents the product at lower magnification. Some of the nanospheres are also

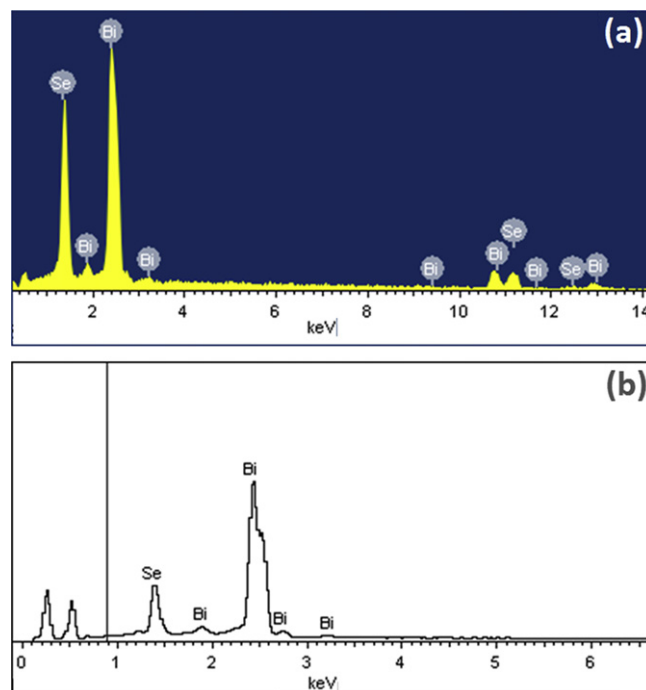
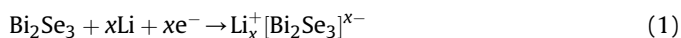


Fig. 2. (a) EDS results of BRNS (b) EDS results of SANS.

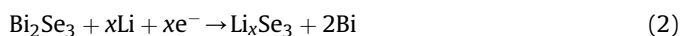
observed in the micrographs Fig. 4(c), these nanospheres also comprise of self assembled nanosheets. Fig. 4(d) shows the morphology of a single sphere consisting of nanosheets.

Fig. 5 presents electrochemical performance at  $50 \text{ mA g}^{-1}$  current density of as synthesized products by thermochemical reaction and by hydrothermal technique respectively. Fig. 5(a) shows the charge discharge curves for the BRNS synthesized by CVD using Bi and Se powders as precursors. It can be depicted from the figure that 1st cycle discharge capacity for BRNS is  $725.6 \text{ mAh g}^{-1}$  and reversible charge capacity is  $521 \text{ mAh g}^{-1}$ , while the 1st cycle discharge capacity for SANS is  $419.4 \text{ mAh g}^{-1}$  and reversible charge capacity is  $347.2 \text{ mAh g}^{-1}$  as presented in Fig. 4(b). Similarly the difference of charge and discharge capacity is observed for the preceding cycles in both cases. It is also evident from the figure that potential slope is quite enormous for the first cycle discharge capacity in the range  $1.7\text{--}0.85 \text{ V}$  which is considered to be due to the following conversion reactions.

Lithium intercalation



Replacement reaction



Two plateaus at  $1.7$  and  $0.85 \text{ V}$  were observed during the discharge due to the lithium potential of  $\text{Li}_x\text{Se}_3$ . Therefore, we suggest two different reactions by which lithium interacts with bismuth selenide. First one is the lithium intercalation in which lithium resides among the quintuple layers of the bismuth selenide; other one is replacement reaction in which lithium replaces bismuth chemically. The charge–discharge profiles for both the samples look like same but discharge capacity suddenly drops to  $419.4 \text{ mAh g}^{-1}$  in case of SANS just after this potential slope. Selenium vacancies and modified surface states are considered to be responsible for this sudden decrease because of the different synthesis technique. The EDS results (Fig. 2) also confirm that extra selenium is present in BRNS due to the methodology adopted.

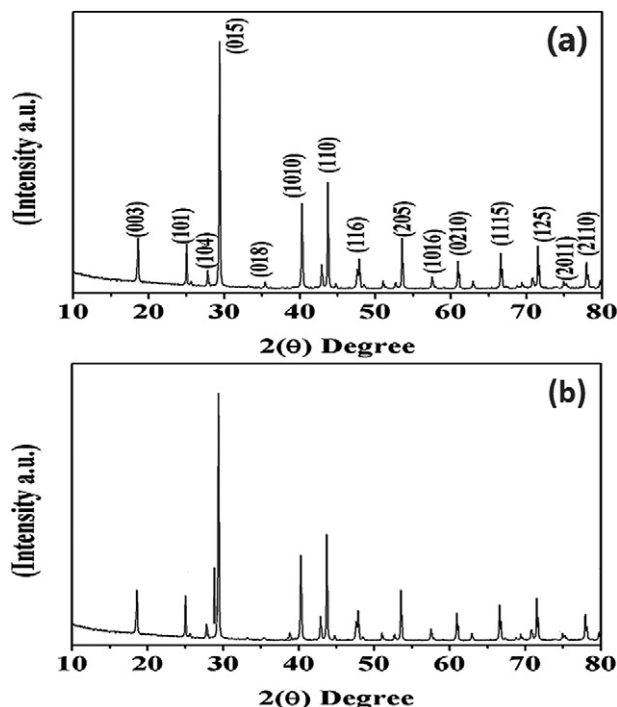
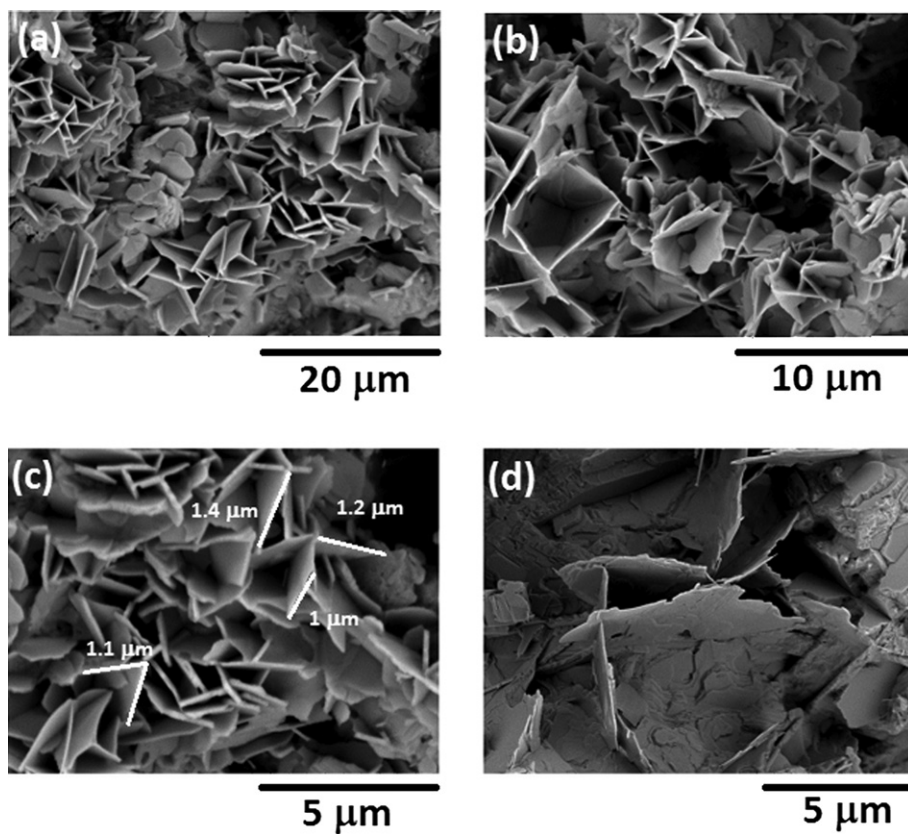
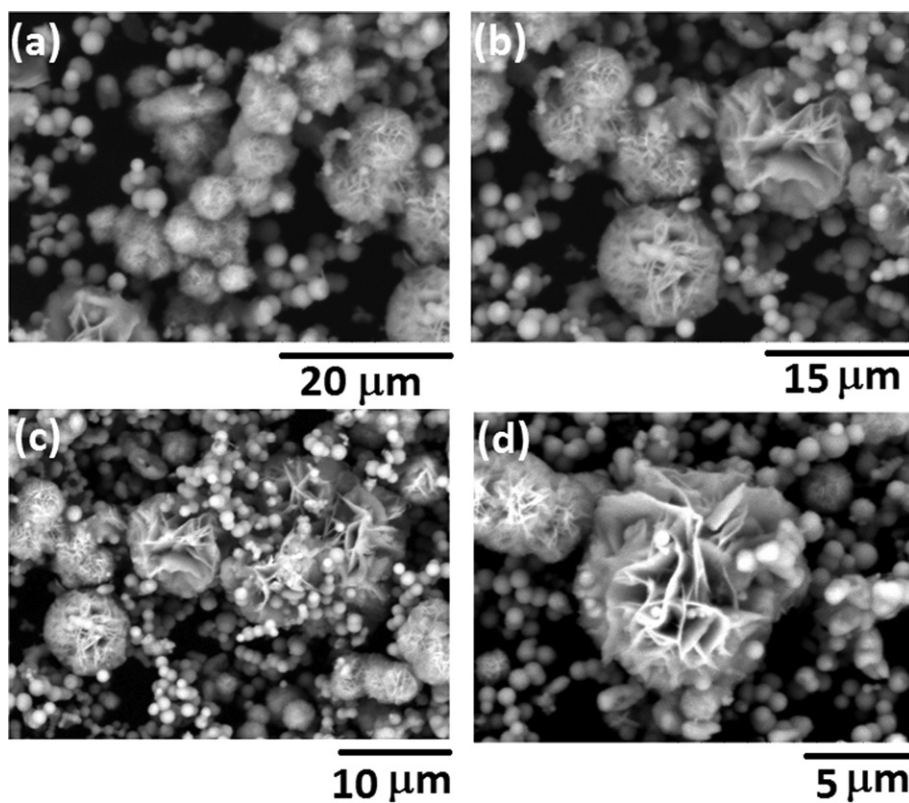


Fig. 1. (a) XRD spectrum of BRNS (b) XRD pattern of SANS.



**Fig. 3.** SEM micrographs of as synthesized  $\text{Bi}_2\text{Se}_3$  nanosheets (BRNS) synthesized by using Bi and Se powders as precursors.



**Fig. 4.** SEM micrographs of as synthesized self assembled nanosheets (SANS) prepared by conventional hydrothermal technique.

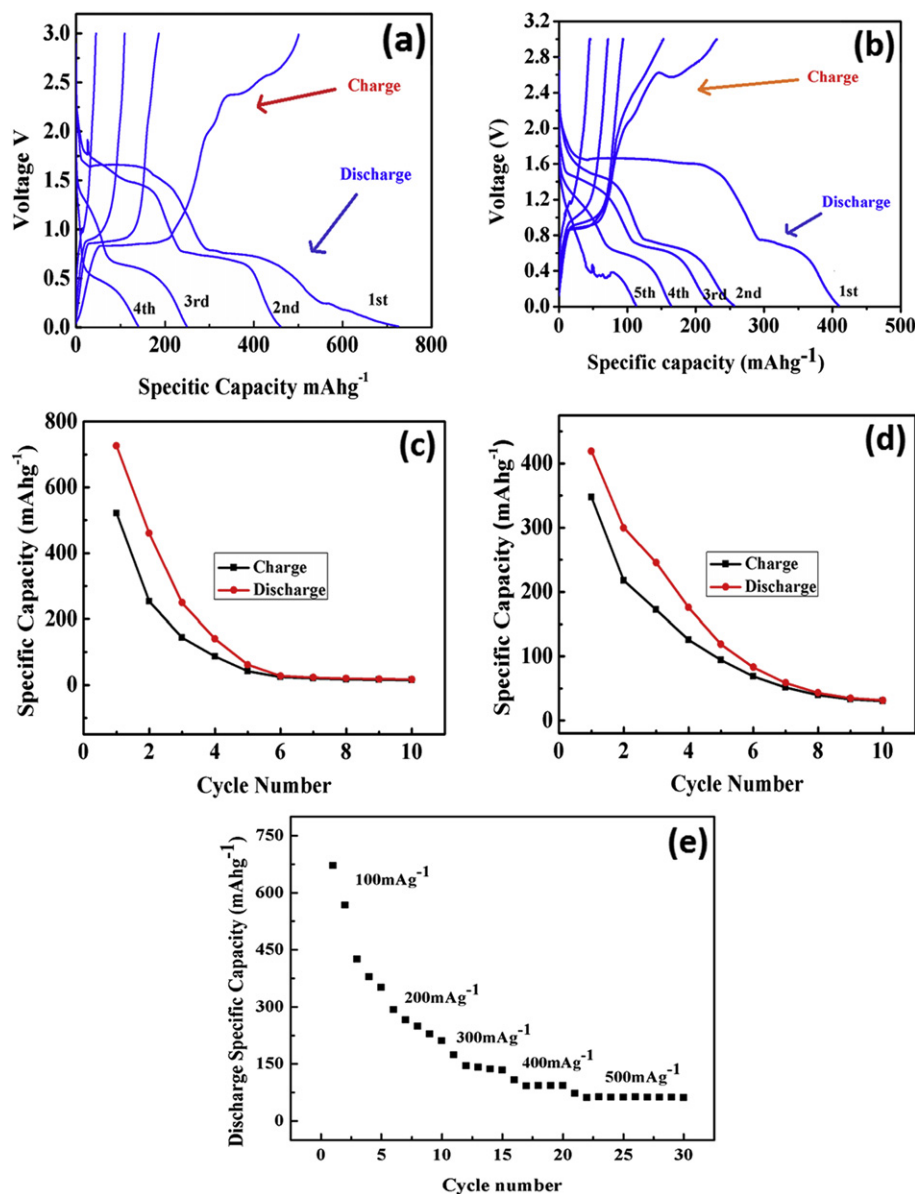


**Fig. 5.** Electrochemical performance of  $\text{Bi}_2\text{Se}_3/\text{Li}$  cells (a) charge/discharge curves of BRNS (b) charge/discharge curves of SANS (c) cyclic performance of BRNS (d) cyclic performance of SANS (e) rate performance of  $\text{Bi}_2\text{Se}_3$ .

Fig. 5(c) shows the cyclic performance of BRNS and (d) represents the cyclic performance of SANS. The comparative study of cyclic performance shows that the slope in case of BRNS is steeper than in case of SANS. Self assembled nanosheets fabricated by hydrothermal technique seem to have better performance in the 2nd and 3rd cycles but after 10 cycles, both the products showed same behavior. The final discharge capacity for both the products drops to  $43 \text{ mAh g}^{-1}$  after 10 cycles and sustains at a value of  $34 \text{ mAh g}^{-1}$  after 50 cycles. Fig. 5(e) represents the rate performance of bismuth selenide which indicates the rate capability of ( $\sim 690, 298, 183, 108$  and  $65 \text{ mAh g}^{-1}$  at  $100, 200, 300, 400$  and  $500 \text{ mA g}^{-1}$  respectively). The technique we have employed seems to be greatly enhancing the initial cycle electrochemical performance of the  $\text{Bi}_2\text{Se}_3$  nanosheets. Although the electrochemical performance is not very high but it can be improved by alloying  $\text{Bi}_2\text{Se}_3$  with other anode materials like  $\eta\text{-Fe}_2\text{O}_3$  or some other materials with the same electrochemical potential.

Bismuth selenide have the hexagonal layered structure: each single layer comprising five atoms thick covalently bonded stacks of  $\text{Se}^1\text{—Bi—Se}^2\text{—Bi—Se}^1$ , and different quintuple layers connected by weak van der Waals bonds. This structure makes it possible to intercalate small atoms into the van der Waals bonded interlayer [34–38]. Equation (1) represents the possible lithium intercalation of bismuth selenide with lithium. From the thermodynamic point of view, there is the prospect for a replacement reaction to occur between lithium and bismuth selenide, which results to the generation of Bi and  $\text{Li}_x\text{Se}$ . There is another aspect from kinetic point of view, for the occurrence of such replacement reaction between lithium and bismuth selenide, there has to be enough energy provided for lithium ions and electrons to destroy original bonds between Bi and Se within the quintuple layer. This energy is provided by constant current density in our case. This replacement reaction is presented in Equation (2). Hence, we suggest two possibilities for chemical reaction of lithium with bismuth selenide,

one is the intercalation to form  $\text{Li}_x^+[\text{BiSe}]^{x-}$  and the other is replacement reaction to form  $\text{Li}_x\text{Se}_3$ .

The amount of lithium which intercalates in bismuth selenide to form the  $\text{Li}_x^+[\text{BiSe}]^{x-}$  or replaces Bi from  $\text{Bi}_2\text{Se}_3$  is very important because it controls the specific charge discharge capacities of the battery. In case of SANS the intercalated lithium amount is low as compared to BRNS. Since SANS are fabricated through conventional hydrothermal technique, the amount of Se present in this sample is naturally low as compared to BRNS which are fabricated by CVD method by using Bi and Se powders as precursors. Therefore we suggest that more Se vacancies are present in SANS as compared to BRNS. This presence of Se vacancies limits the value of intercalated Li in the case of SANS hence reducing their specific discharge capacity. Very little or no Se vacancies in BRNS increase the specific discharge capacity of BRNS by increasing the amount of intercalated lithium. This fact is also evident by EDS analysis presented in Fig. 2, which indicates low stoichiometric ratio of Se in SANS as compared to BRNS.

The cyclic efficiency of the batteries depend upon the reversible reaction i.e. exfoliation of lithium ions. The exfoliation of Li ions from  $\text{Li}_x^+[\text{BiSe}]^{x-}$  in both cases is low therefore, reducing the cyclic capacity of the sample. Here is the need to focus the research attention, because if cyclic performance can be increased by making alloys with bismuth selenide to exfoliate the amount of lithium, this material could serve as the advanced lithium ion battery material.

The possible reason for low cyclic efficiency or capacity fading is presented in Equation (1) which we state lithium Intercalation and is held responsible for cyclic efficiency in our case. Since bismuth selenide has a layered structure in which these layers are bonded by weak Van der-Waals forces, such structure allows the lithium to intercalate or reside in between the quintuple layers as shown in the Fig. 6 below. This is worth mentioning here that this process is highly reversible i.e. the intercalated lithium can also be recovered by applying the potential very easily. In our case the amount of intercalated lithium is small which reduces the recovered amount of lithium for the next cycle as well. As a result the cyclic efficiency of the battery is reduced.

The second process is replacement reaction which is supposed to be the major cause of reducing the life performance. This chemical reaction is not reversible, so the major part of the lithium is consumed by this chemical reaction forming  $\text{Li}_x\text{Se}_3$  in the first cycle. So the first cycle capacity is high in both samples. For the second cycle not much amount of lithium is present for this irreversible reaction to take place. This chemical reaction diminishes very rapidly with the number of cycle as a result specific capacity decreases in second cycle and so on. Up to the 10th cycle this reaction almost dies out and remaining process is only the intercalation and exfoliation of the lithium which is highly reversible

process. As a result the specific capacity decreases to  $34 \text{ mA g}^{-1}$  and becomes almost stable at this point even up to 50 cycles.

Second reason is the formation of solid-electrolyte interface (SEI) layer on the anode surface. The energy gap ( $E_g$ ) between the lowest unoccupied molecular orbital (LUMO) and the highest occupied molecular orbital (HOMO) of an electrolyte is the window of the electrolyte. The electrochemical potentials of charged cell need to be matched to the LUMO and HOMO of the electrolyte. If the Fermi energy of a solid anode is above the LUMO of the electrolyte, the anode will reduce the electrolyte forming a SEI passivation layer. Since electrochemical potential of bismuth selenide is greater than LUMO, a SEI layer of  $\text{Li}_x\text{Se}_3$  as a result of irreversible reaction is formed on anode surface reducing the specific capacity in the next cycles.

The cyclic efficiency of bismuth selenide alone in batteries is not very good or capacity fading is relatively high, so we suggest that this material will show interesting results with other well performing materials as composite. To improve the electrochemical kinetics, the electrode materials need to be embedded within an electronically conducting species. Furthermore, the internal electrical field generated by electrons may enhance the ionic motions. Such modifications diminish the problem of low electronic conductivity, at the same time, reducing the size of active material would shorten the diffusion length for lithium. The combination of such nanostructured composites consisting of thermoelectric materials and conductive additives will makes it possible to enhance capacities at intermediate or even higher rates.

Electrode materials must fulfill two fundamental requirements to reach the goal of a high specific energy and energy density: (a) a high specific charge and charge density, that is, a high number of available charge carriers per mass and volume unit of the material; (b) a high reversibility of electrochemical reactions at both electrodes to maintain the specific charge for high number of charge–discharge cycles. These two requirements can be fulfilled by using the composite of bismuth selenide and iron oxide nanostructures.

Now, since  $\text{Bi}_2\text{Se}_3$  is layered material and the fundamental geometrical transitions of layered material lattice matrices upon intercalation of lithium include: (1) change in interlayer spacing, (2) change in stacking mode of the layers, and (3) formation of intermediate phases at low lithium concentrations. Ion exchange is a method to replace the guest ion in an intercalation compound with another guest ion, which offers a useful route for intercalating large ions that do not intercalate directly.

#### 4. Conclusion

In conclusion, we have successfully synthesized the  $\text{Bi}_2\text{Se}_3$  nanosheets by different synthesis approaches and compared the electrochemical performance of the material for the first time. Although, there have been no reports on the electrochemical

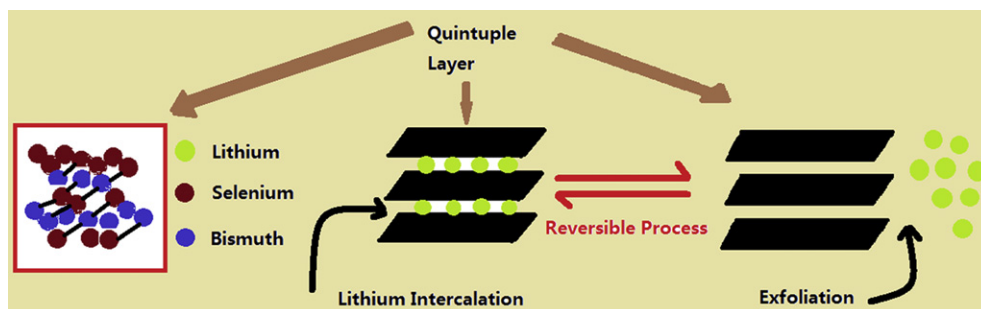


Fig. 6. Schematic presentation of lithium intercalation.

performance of this material because it has been considered a poor material for lithium ion batteries applications. This kind of material was intentionally selected due to its excellent thermoelectric properties. The first discharge capacity has greatly improved from 419.4 mAh g<sup>-1</sup> to 725.6 mAh g<sup>-1</sup>. Similarly reversible capacity retention has been improved from 347.2 mAh g<sup>-1</sup> to 521 mAh g<sup>-1</sup>. The results clearly suggest that with the slight exploitation in the existing synthesis approach can greatly enhance the potential properties of the materials for application in lithium ion batteries. We come to the conclusion that only using this material in lithium batteries will not be advantageous because cycling efficiency is low so we suggest it can be used as composite with some well performing materials in order to enhance the thermoelectric properties of batteries. We recommend that further work must be carried out on bismuth selenide as this material has a great potential for applications in advanced batteries.

### Acknowledgment

This work was supported by National Natural Science Foundation of China (20471007, 50972017) and the Research Fund for the Doctoral Program of Higher Education of China (20101101110026).

### References

- [1] Qingsong Wanga, Ping Pinga, Xuejuan Zhaoa, Guanquan Chub, Jinhua Suna, Chunhua Chen, J. Power Sources 208 (2012) 210–224.
- [2] A. Hammami, N. Raymond, M. Armand, Nature 424 (2003) 635–636.
- [3] Hongmei Cui, Hong Liu, Xia Li, Jiyang Wang, Feng Han, Xudong Zhang, R.I. Boughton, J. Solid State Chem. 177 (2004) 4001–4006.
- [4] Arup Purkayastha, Abhishek Jain, Claudiu Hapenciuc, Rok Buckley, Binay Singh, C. Karthik, Rutvik J. Mehta, Theodorian Borca-Tasciuc, Ganpati Ramanath, Chem. Mater. 23 (2011) 3029–3031.
- [5] Jipeng Fu, Shuyan Song, Xiaoguang Zhang, Feng Cao, Liang Zhou, Xiyan Li, Hongjie Zhang, Cryst. Eng. Commun. 14 (2012) 2159–2165.
- [6] N.S. Patil, A.M. Sargar, S.R. Maneb, P.N. Bhosaleb, Mater. Chem. Phys. 115 (2009) 47–51.
- [7] Cham Kim, Dong Hwan Kim, Yoon Soo Han, Jong Shik Chung, SangHa Park, Soonheum Park, Hoyoung Kim, Mater. Res. Bull. 46 (2011) 407–412.
- [8] Anuja Datta, Jagannath Paul, Arik Kar, Amitava Patra, Zhengliang Sun, Lidong Chen, Joshua Martin, George S. Nolas, Cryst. Growth Des. 10 (2010) 3983–3989.
- [9] Clarence Anglin, Nathan Takas, Juan Callejas, Pierre F.P. Poudeu, J. Solid State Chem. 183 (2010) 1529–1535.
- [10] Lykourgos Iordanidis, Paul W. Brazis, Theodora Kyratsi, John Ireland, Melissa Lane, Carl R. Kannewurf, Wei Chen, Jeffrey S. Dyck, Ctirad Uher, Nishant A. Ghelani, Tim Hogan, Mercouri G. Kanatzidis, Chem. Mater. 13 (2001) 622–633.
- [11] L.D. Hicks, M.S. Dresselhaus, Phys. Rev. B 47 (1993) 12727.
- [12] L.D. Hicks, M.S. Dresselhaus, Phys. Rev. B 47 (1993) 16631.
- [13] L.D. Hicks, T.C. Harman, X. Sun, M.S. Dresselhaus, Phys. Rev. B 53 (1996) 10493.
- [14] T.C. Harman, P.J. Taylor, D.L. Spears, M.P. Walsh, J. Electron. Mater. 29 (2000) L1–L4.
- [15] M. Tritt, Science 283 (1999) 804.
- [16] R. Venkatasubramanian, E. Siivola, T. Colpitts, B. Quinn, Nature 413 (2001) 597.
- [17] H.T. El-Shair, A.M. Ibrahim, E.A. El-Wahabb, M.A. Afify, F.A. El-salam, Vacuum 42 (1991) 911.
- [18] Zhengliang Sun, Shengcong Liufu, Xihong Chena, Lidong Chena, Chem. Commun. 46 (2010) 3101–3103.
- [19] Lianshan Li, Ruiguo Cao, Zhijian Wang, Jingjian Li, Limin Qi, J. Phys. Chem. C 113 (2009) 18075–18081.
- [20] S.K. Mishra, S. Satpathy, O. Jepsen, J. Phys. Condens. Matter 9 (1997) 461.
- [21] Jun Li, Yongchun Zhu, Jin Du, Junhao Zhang, Yitai Qian, Solid State Commun. 147 (2008) 36–40.
- [22] Pengfei Hu, Yali Cao, Dianzeng Jia, Luxiang Wang, Mater. Lett. 64 (2010) 493–496.
- [23] Desheng Kong, Judy J. Cha, Keji Lai, Hailin Peng, James G. Analytis, Stefan Meister, Yulin Chen, Hai-Jun Zhang, Ian R. Fisher, Zhi-Xun Shen, Yi Cui, ACS Nano 5 (2011) 4698–4703.
- [24] Y. Jiang, Y.J. Zhu, G.F. Cheng, Cryst. Growth Des. 6 (2006) 2174–2176.
- [25] X.F. Qiu, C. Burda, R.L. Fu, L. Pu, H.Y. Chen, J.J. Zhu, J. Am. Chem. Soc. 126 (2004) 16276–16277.
- [26] A. Jagminas, I. Valsiūnas, G.P. Veronese, R. Juškėnas, A. Rutavičius, J. Cryst. Growth 310 (2008) 428–433.
- [27] Youyong Liu, Chuanbao Cao, Jing Li, Xingyan Xu, J. Appl. Electrochem. 40 (2010) 419–425.
- [28] Peichao Liana, Xuefeng Zhu, Shuzhao Lianga, Zhong Li, Weishen Yangb, Haihui Wang, Electrochim. Acta 56 (2011) 4532–4539.
- [29] J.M. Yan, H.Z. Huang, J. Zhang, Z.J. Liu, Y. Yang, J. Power Sources 146 (2005) 264–269.
- [30] Z.P. Xia, Y. Lin, Z.Q. Li, Mater. Charact. 59 (2008) 1324–1328.
- [31] H. Liu, H.M. Cui, F. Han, X. Li, J.Y. Wang, R.I. Boughton, Cryst. Growth Des. 5 (2005) 1711–1714.
- [32] S.K. Batabyal, C. Basu, A.R. Das, G.S. Sanyal, Mater. Lett. 60 (2006) 2582–2585.
- [33] X.H. Yang, X. Wang, Z.D. Zhang, J. Cryst. Growth 276 (2005) 566–570.
- [34] J. Bludská, S. Karamzov, J. Navratil, J. Horak, Solid State Ion. 171 (2004) 251–259.
- [35] J.K. Chen, Z.L. Sun, Y.J. Zhu, N.F. Chen, Y.F. Zhou, J. Ding, X.H. Chen, L.D. Chen, Dalton Trans. 40 (2011) 340–343.
- [36] Z.F. Ding, L. Viculis, J. Nakawatase, R.B. Kaner, Adv. Mater. 13 (2001) 797–800.
- [37] Z.F. Ding, S.K. Bux, D.J. King, F.L. Chang, T.H. Chen, S.C. Huang, R.B. Kaner, J. Mater. Chem. 19 (2009) 2588–2592.
- [38] Jikun Chen, Yingjie Zhu, Nuofu Chen, Xinling Liu, Zhengliang Sun, Zhenghong Huang, Feiyu Kang, Qiuming Gao, Jun Jiang, Lidong Chen, J. Nanopart. Res. 13 (2011) 6569–6578.